TECHNICAL BRIEF

Key Points:
- This is a uniform shear wave splitting database for western and central US
- It contains 16,105 pairs of shear wave splitting measurements
- Systematic spatial variations are observed

Supporting Information:
- Readme
- Tables S1–S3

Correspondence to:
K. H. Liu,
liukh@mst.edu

A uniform database of teleseismic shear wave splitting measurements for the western and central United States

Kelly H. Liu[1], Ahmed Elsheikh[1], Awad Lemnifi[1], Uranbaigal Purevsuren[1], Melissa Ray[1], Hesham Refayee[1,2], Bin B. Yang[1], Youqiang Yu[1], and Stephen S. Gao[1]

[1]Geology and Geophysics Program, Missouri University of Science and Technology, Rolla, Missouri, USA, [2]Now at dGB Earth Sciences, Sugar Land, Texas, USA

Abstract We present a shear wave splitting (SWS) database for the western and central United States as part of a lasting effort to build a uniform SWS database for the entire North America. The SWS measurements were obtained by minimizing the energy on the transverse component of the PKS, SKKS, and SKS phases. Each of the individual measurements was visually checked to ensure quality. This version of the database contains 16,105 pairs of splitting parameters. The data used to generate the parameters were recorded by 1774 digital broadband seismic stations over the period of 1989–2012, and represented all the available data from both permanent and portable seismic networks archived at the Incorporated Research Institutions for Seismology Data Management Center in the area of $26.00°N$ to $50.00°N$ and $125.00°W$ to $90.00°W$. About 10,000 pairs of the measurements were from the 1092 USArray Transportable Array stations. The results show that approximately 2/3 of the fast orientations are within $30°$ from the absolute plate motion (APM) direction of the North American plate, and most of the largest departures with the APM are located along the eastern boundary of the western US orogenic zone and in the central Great Basins. The splitting times observed in the western US are larger than, and those in the central US are comparable with the global average of 1.0 s. The uniform database has an unprecedented spatial coverage and can be used for various investigations of the structure and dynamics of the Earth.

1. Introduction

Shear wave splitting (SWS) analysis has recently evolved into one of the most frequently used tools in structural seismology to delineate finite strain in the lithosphere and asthenosphere [*Fuchs*, 1977; *Ando et al.*, 1983; *Silver and Chan*, 1991; *Vinnik et al.*, 1992; *Silver*, 1996]. It takes the advantage of the fact that when a shear wave encounters anisotropic layers, it splits into two orthogonally polarized waves propagating at different speed. The splitting parameters, which include the polarization orientation of the fast wave (fast orientation) and the delay time between the fast and slow waves (splitting time), have been widely used to understand mantle anisotropy and dynamics. The most commonly utilized shear waves for SWS are P-to-S converted waves at the core-mantle boundary on the receiver side, mostly PKS, SKKS, and SKS (hereafter collectively called XKS). The steep angle of incidence of the XKS phases and the known initial polarization orientation (which is parallel to the back-azimuth of the event) make the XKS phases ideal for investigating anisotropic structures beneath the receivers.

As summarized in numerous previous studies, mostly due to the diversity in the SWS parameter measuring techniques, data selection standards, and result ranking criteria used by different research groups, significant discrepancies were frequently found in previous studies [e.g., *Vecsey et al.*, 2008; *Liu et al.*, 2008]. Our first attempt to create a uniform database at a continental scale led to the publication of NA-SWS-1.1, the first uniform SWS database for North America [*Liu*, 2009]. NA-SWS-1.1 provides 6224 pairs of SWS parameters for the entire North America (and 3391 pairs for western and central United States) using data archived at the IRIS (Incorporated Research Institutions for Seismology) DMC (Data Management Center) and recorded by 850 permanent and portable seismic stations during the period of 1987–2007 (Figure 1). Since then a tremendous amount of data have been recorded by existing stations and newly deployed stations. Undoubtedly, in North America, the area with the greatest increase in spatial coverage is the western and central United States, mostly due to the commencement of the USArray Transportable Array stations in the area. NA-SWS-1.1 only used the SKS phase. Previous studies suggested that the addition of the SKKS and
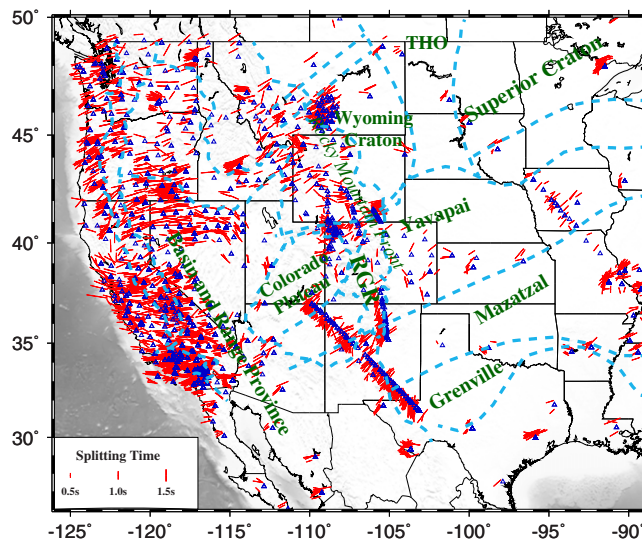
Figure 1. Map showing 3391 pairs of SKS shear wave splitting measurements in the NA-SWS-1.1 database for western and central United States. The values are plotted at the surface projections of the ray-piercing points at the depth of 200 km. The orientation of the red bars represents the polarization orientation of the fast wave, and the length is proportional to the splitting time. The dashed lines are the boundaries of major tectonic or basement provinces. THO = Trans-Hudson Orogeny; RGR = Rio Grande Rift.

PKS phases could increase both the number of SWS measurements at a station and the azimuthal coverage of the XKS events, making it possible for investigating complex anisotropy [e.g., *Gao and Liu*, 2009; *Gao et al.*, 2010].

Here we report the results of a multiyear effort to remeasure XKS splitting parameters for the western and central United States (WCUS). The SWS database (Figure 2) contains 16,105 pairs of SWS parameters and represents an approximately fivefold increase in the number of measurements for the WCUS over NA-SWS-1.1. The individual measurements are presented as an electronic supporting information (Table S1), together with station-averaged (Table S2) and area-averaged (Table S3) SWS parameters. The individual and station-averaged data sets and related plots can be found from the IRIS DMC as a data product at http://www.iris.edu/dms/products/sws-db-mst/.

2. Data Used to Produce the Database

This version of SWS database uses all the available broadband seismic data archived at the IRIS DMC, from teleseismic events occurred between 1989 and 2012. Due to the approximately 2 year duration of the project, data from some of the stations ended earlier than December 2012. The missing data will be added in future revisions of the database. The study area is in the range of 26.00°N to 50.00°N and 125.00°W to 90.00°W. The seismic stations contributed to the database belong to a number of seismic networks, including the USArray Transportable Array (network code TA), IRIS/USGS Global Seismographic Network (IU), the US National Seismic Network (US), GEOSCOPE (G), and PASSCAL portable seismic arrays.

We use XKS data from events with magnitude ≥ 5.6, which is reduced to 5.5 if the focal depth is >100 km to take advantage of sharper waveforms. The epicentral distance ranges are 84°–180° for SKKS and SKS, and 120°–180° for PKS. The seismograms were detrended and band-pass filtered in the frequency range of 0.04–0.5 Hz which contains the main

Figure 2. Map showing 16,105 pairs of XKS shear wave splitting measurements in the database plotted at the surface projection of the ray-piercing points at the depth of 200 km. Stations are shown as triangles.
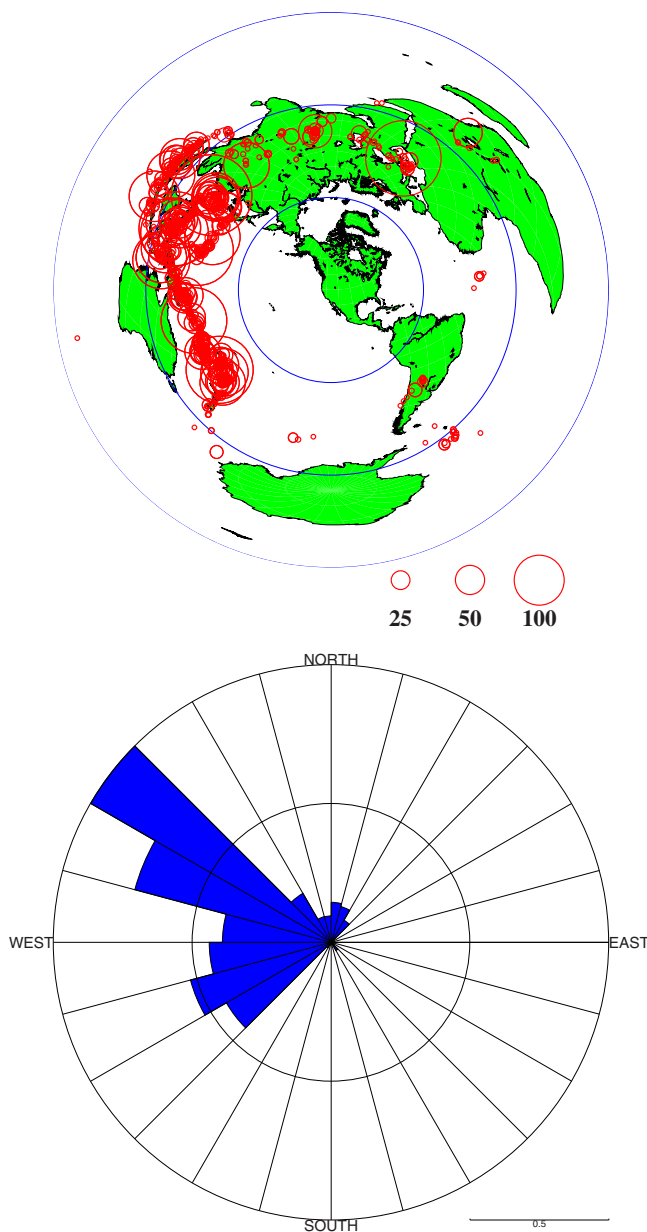
Figure 3. (top) An azimuthal equidistant projection map showing the distribution of earthquakes used in the study. The size of a circle is proportional to the number of SWS measurements that the event provided. (bottom) A rose diagram showing the distribution of the back azimuth of the events.

XKS energy. The distribution of the earthquakes used in the study is shown in Figure 3.

3. Measuring Procedure

To measure the SWS parameters, we utilized the minimization of energy on the transverse component approach [*Silver and Chan*, 1991], which is arguably the most commonly used and the most stable one when noise is present [*Vecsey et al.*, 2008]. The technique searches for the optimal pair of SWS parameters that most effectively remove the energy on the transverse component. The procedure for measuring and ranking SWS parameters consists of several steps, and is a combination of automated processing and manual screening and adjustments. Detailed information about the measuring and ranking procedure can be found in *Liu et al.* [2008], *Liu* [2009], and *Liu and Gao* [2013], and is briefly summarized below.

In the procedure, an automatic data selection procedure was first applied to the band-pass filtered seismograms to remove waveforms with low XKS energy on the radial component. The selected XKS waveforms were automatically windowed based on the theoretical arrival times, and the splitting parameters were measured using the method of *Silver and Chan* [1991]. The resulting measurements were ranked as A (outstanding), B (good), C (poor), and N (Null) based on the S/N ratio on the original and corrected radial and transverse components [*Liu et al.*, 2008]. All of the individual SWS parameters were then visually screened to optimize the start and end times of the XKS window, adjust the filtering parameters, and verify and modify if necessary the quality ranking. We found that while it was frequently necessary to adjust the start and end times of the XKS window and the quality ranking, adjusting the corner frequencies was rarely needed, probably due to the excellent site conditions for most of the stations.

Null measurements are the results of absence of XKS energy on the original transverse component. Such an absence can be caused by a lack of net anisotropy along the raypath from the core mantle boundary to the station and is also observed when the back-azimuth of an event is parallel or orthogonal to the fast orientation. As argued and demonstrated using synthetic data in *Liu and Gao* [2013], in
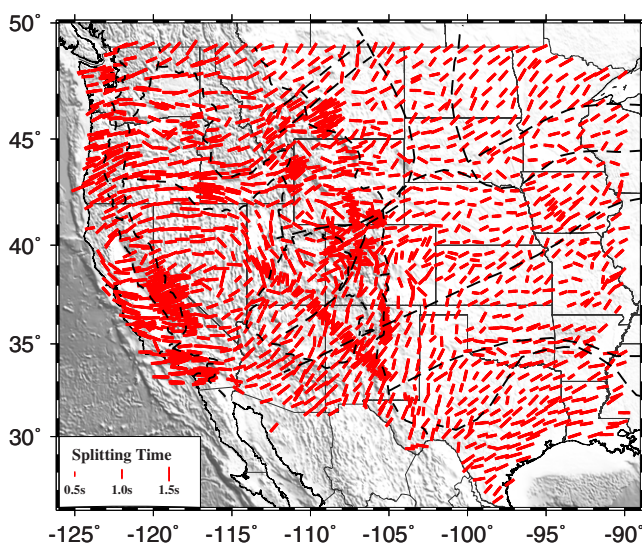
Figure 4. Station-averaged shear wave splitting measurements. The averaged fast orientation of a given station was calculated by the circular mean of the individual fast orientations from the station, and the averaged splitting times were produced by averaging the individual splitting times.

practice it is difficult to objectively judge the presence of XKS energy on the transverse component because all the seismograms contain noise. Strictly speaking, a pure lack of XKS energy on the original transverse component does not exist, due to factors such as finite source size, scattering, off great circle arrivals, undetected sensor misorientation, and departure from a perfect single layer of anisotropy with a horizontal axis of symmetry. Thus, the determination of a Null measurement is subjective and sometimes even arbitrary, often leading to excessive use of the Null ranking [*Liu and Gao*, 2013]. Therefore, while we do not completely exclude the chance of including Null or near-Null measurements in future versions of the database, the current version only contains quality A and B measurements.

4. Contents of the Databases

More than 100,000 three-component seismograms were visually checked and a total of 16,105 pairs of quality A and B measurements were obtained (Figure 2). The total number of measurements for PKS, SKKS, and SKS is 1407, 2451, and 12,247, respectively.
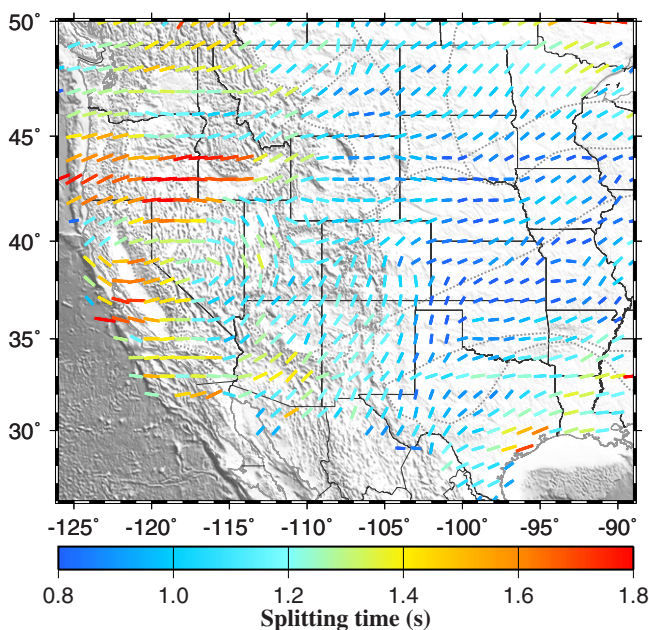
Figure 5. Spatially averaged (in radius=1° circles) shear wave splitting parameters. The color of the bars represents the splitting time.

The resulting database is presented in three forms, including (1) individual SWS measurements from each of the event-station pairs (Figure 2 and Table S1); (2) station-averaged SWS measurements (Figure 4 and Table S2), and (3) area-averaged measurements in overlapping radius=1° circles (Figure 5 and Table S3).

4.1. Individual Measurements
The individual SWS measurement database (Table S1) contains 17 columns. Column 1 is the station name. For the ease of computer processing of the SWS measurements, we created a nine-letter network-aware station naming system. The first six letters represent the station name. If the original name has less than six letters, one or
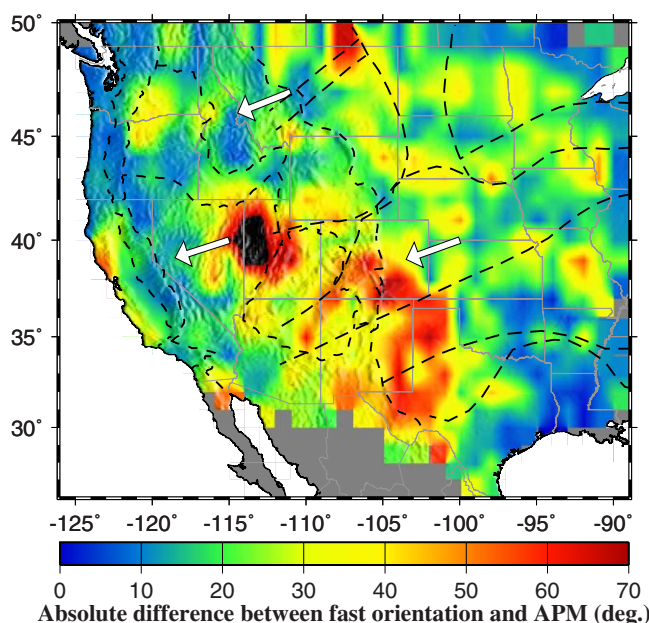
Figure 6. Absolution differences between the fast orientations and absolute plate motion (APM) directions of the North American plate determined by the HS3-NUVEL1A model [*Gripp and Gordon*, 2002]. The white arrows represent the APM directions of the North American plate.

more lower-case x's are added at the end of the name so that all the stations have six-letter names. The last two letters are network code and is padded by a "y" if the network code is single lettered.

Column 2 gives the phase name including PKS, SKKS, or SKS, and Column 3 is the event name. The events are named as EQyydddhhmm where yy is the year, ddd is the day of the year, hh is the hour, and mm is the minute of the origin time (universal time). Columns 4 and 5 are the latitude and longitude of the station in degrees, and Columns 6 and 7 give the fast polarization orientation (measured clockwise from the north) and its standard deviation in degree. Columns 8 and 9 are the splitting time and its standard deviation in second.

Column 10 is the back-azimuth (BAZ) of the event relative to the station measured clockwise from the north. Column 11 gives the modulo-90° of the BAZ. BAZ90 = BAZ when BAZ is between 0 and 90°; BAZ-90° when BAZ is between 90° and 180°; BAZ-180° when BAZ is in the range of 180° and 270°; and BAZ-270° when BAZ is >270°. BAZ90 is particularly useful for recognizing and modeling anisotropic structures with a $\pi/2$ periodicity such as multiple horizontal layers [*Silver and Savage*, 1994; *Yang et al.*, 2014].

Columns 12, 13, and 14 contain the latitude and longitude (in degree) of the epicenter and the focal depth (in km). Column 15 gives the quality rank of the measurement, and Columns 16 and 17 are the latitude and longitude of the XKS ray-piercing points, computed at the depth of 200 km.

4.2. Station-Averaged Measurements

The vast majority of previous SWS measurements were presented in the form of station-averaged splitting parameters. They can be conveniently used by various kinds of studies when the anisotropic structure beneath the station is laterally uniform and is single-layered with a horizontal axis of symmetry. The database of station-averaged SWS parameters (Figure 4 and Table S2) has the following columns: station name, latitude, longitude, fast polarization orientation and its standard deviation, splitting time and its standard deviation, and the number of individual measurements involved in the calculation.

4.3. Area-Averaged Measurements

Station-averaged splitting parameters (Figure 4) are not evenly spaced, resulting in uneven weighting factors when they are used for future studies. To produce a spatially evenly spaced SWS database, we averaged individually measurements with piecing points (at the depth of 200 km) in R = 1° circles. The distance between the neighboring circles is 1°, thus there is an overlap between the circles. The resulting spatial distribution of SWS measurements shows systematic variations (Figure 5). Given the large amount of individual measurements from the densely spaced stations, SWS measurements are found in all of the circles in WCUS, resulting in a continuous coverage of the entire study area. The database (Table S3) contains seven columns, including the latitude and longitude of the center of the circles, fast polarization orientation and its standard deviation, splitting time and its standard deviation, and the number of individual measurements involved in the calculation.
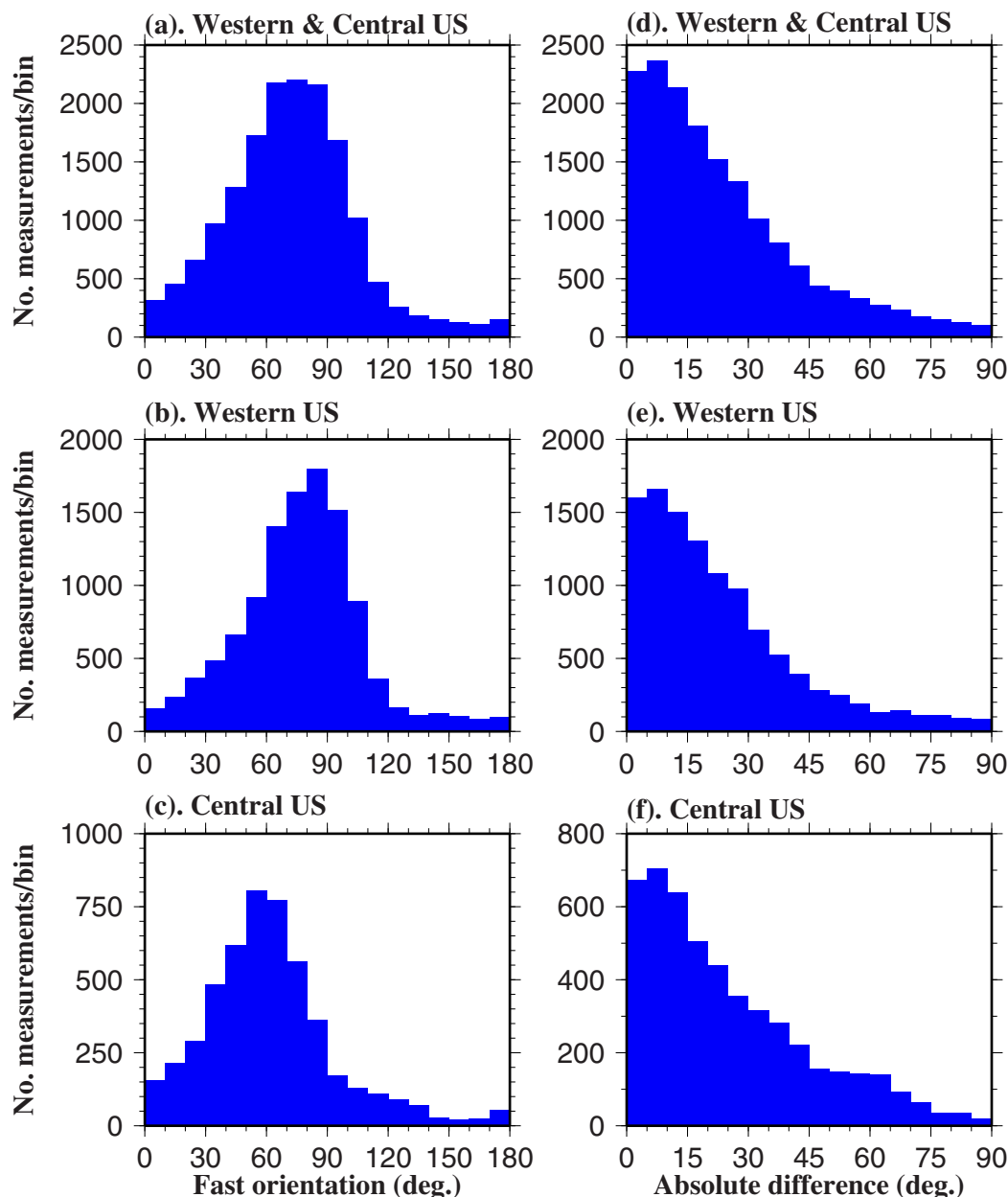
Figure 7. (a–c) Histograms of fast orientations and (d–f) the absolute difference between the fast orientations and the North American APM. (top) Results for the entire study area, (middle) the area west of 105°W, and (bottom) the area east of 105°W.

5. Spatial and Azimuthal Distributions of SWS Parameters

The database shows systematic spatial variations of the splitting parameters, which vary systematically with the BAZ in some areas and suggest the existence of complex anisotropy. In the following, we summarize these major features without attempting to speculate much on the geodynamic implications.

5.1. Fast Orientations

To explore spatial correspondence between the observed fast orientations and the direction of absolute plate motion (APM), we compute the APM direction for North America based on the HS3-NUVEL1A model [*Gripp and Gordon*, 2002] at each of the 16,105 XKS ray-piercing points, and obtain the absolute difference between the APM direction and fast orientation in the 0–90° range at each point (Figure 6). The results suggest that for most of the study area (and approximately for 2/3 of the measuring points), the fast orientations are within 30° away from the APM direction of the North American plate (Figure 7). One of the areas
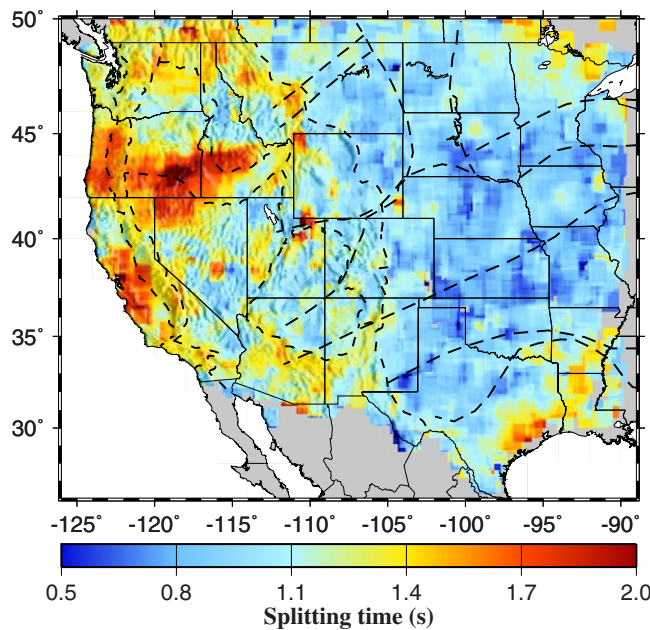
Figure 8. Spatial distribution of the shear wave splitting times. The averaged splitting times are produced by averaging the individual splitting times at piercing points of 200 km deep in overlapping 1° by 1° blocks with a moving step of 0.1°.
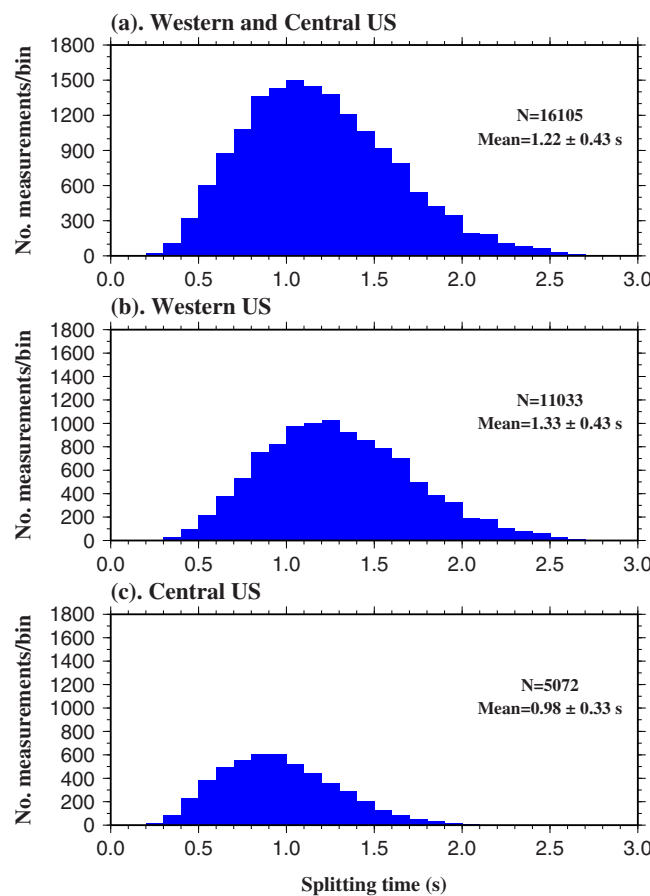
Figure 9. Histograms showing the distribution of the XKS splitting times in (a) the entire study area, (b) western US, and (c) central US.

with exceptions is along the eastern edge of the western US orogenic zone (i.e., the area from the western coast to the Rocky Mountain Front), where the fast orientations are mostly N-S, probably due to the southward mantle flow deflected by the root of the thick lithosphere in the central US [*Refayee et al.*, 2013; *Yang et al.*, 2014]. Another area is located in the central Great Basins, which is the approximate center of a half-circular pattern of fast orientations in the western United States observed previously [*Savage and Sheehan*, 2000; *Silver and Holt*, 2002; *Liu*, 2009].

The consistency between the APM and the fast orientations is especially remarkable in the central US (Figure 7) and is less significant for the western US, mostly due to the half-circular pattern of fast orientations. Furthermore, the correlation length of the fast orientations in the tectonically stable central US seems greater than that of the western US and the area beneath the extended crust north of the Gulf of Mexico, an observation that is consistent with the conclusion of *Becker et al.* [2007] based on a global SWS data set. An in-depth investigation of the mechanisms responsible for the different correlation lengths is beyond the scope of this technical brief.

5.2. Splitting Times

In general, the splitting times west of the Rocky Mountain Front (RMF) are larger than the global mean of about 1.0 s, while those east of the RMF are slightly lower than 1.0 s (Figure 8). Areas with the greatest splitting times are found in southern Oregon, central California, and SE Texas, and the smallest splitting times are located in the central Great Plains. This spatial distribution is
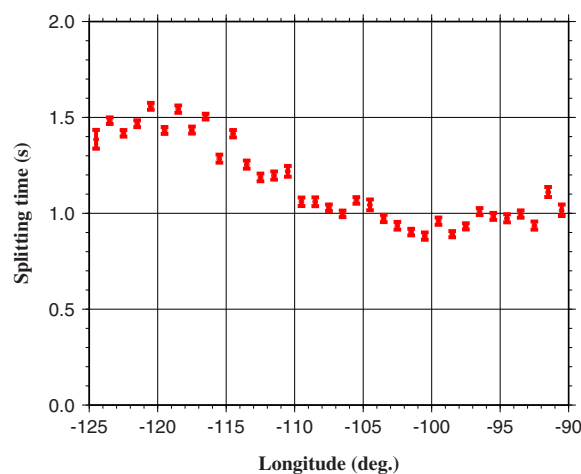
Figure 10. Splitting times averaged over longitudinal bands of 1° wide. A systematic eastward decrease is observed in the western US.

shown in Figure 8, in which the mean splitting time for the entire study area, the area west of 105°W, and that east of 105°W is 1.22 ± 0.43 s, 1.33 ± 0.43 s, and 0.98 ± 0.33 s, respectively (Figure 9). When averaged in N-S bands of 1° wide, the maximum splitting time in the study area is found near 120°W. The splitting times decrease almost linearly eastward in the longitudinal range of 120°W–100°W, from about 1.6 s to about 0.9 s (Figure 10).

5.3. Azimuthal Variations of the Splitting Parameters

Systematic variations of the splitting parameters with the BAZ are diagnostics of complex anisotropy. The most common types of complex anisotropy include two or more layers with a horizontal axis of symmetry, and a single anisotropic layer with a tilt axis. On the splitting parameter versus BAZ plot, the former has a 90° and the latter has a 180° periodicity [*Silver and Savage*, 1994]. With sufficient azimuthal coverage, it is possible to characterize the properties of complex anisotropy [e.g., *Gao and Liu*, 2009; *Yang et al.*, 2014].

To evaluate the spatial distribution of the azimuthal coverage in the study area, we divide the area into overlapping circles with a radius of 0.5°. The distance between neighboring circles is also 0.5°. We then combine the splitting measurements from all the stations in each circle, and count the number of 30°-wide BAZ bins in which the events arrived from. The results suggest that areas with a greater azimuthal coverage have more densely spaced stations and/or stations with a longer period of operation (Figure 11a). A modal value of 2 (out of 12) suggests that the majority of the areas have inadequate azimuthal coverages for reliably identifying and characterizing complex anisotropy (Figure 11b), mostly due to the fact that the vast majority of the events are in a narrow (60°) BAZ range of 245°–305° (Figure 3).

Because complex anisotropy is characterized by azimuthal variations of the splitting parameters especially the fast orientations, we compute the spatial distribution of the circular standard deviation (SD) of the fast orientations from stations in each of the $r = 0.5°$ circles (Figure 12). Areas with the largest SD (and thus the most likely existence of complex anisotropy) are located along the boundary between the active western and stable central US, and along the northern margin of the Yavapai Province beneath which an asthenospheric flow system along a lithospheric channel was proposed by *Yang et al.* [2014]. To test the above preliminary observation, we visually check the azimuthal variation of each of the stations and assign the station a "complex anisotropy index" (CAI). A CAI value of 0 is given to a station if it possesses adequate azimuthal coverage and the splitting parameters do not show a systematic azimuthal variation, and a value of 2 is assigned if a systematic variation is demonstrated. For stations with a poor azimuthal coverage, for which the existence of complex anisotropy cannot be determined, a value of 1 is given to the station [*Yang et al.*, 2014]. The resulting distribution of CAI (Figure 13) is in general agreement with that of the SD (Figure 12), suggesting that the SD of the fast orientations is a good approximation for the existence of complex anisotropy. The majority of the stations showing complex anisotropy have a 90° periodicity [*Yang et al.*, 2014] which is characteristic of multiple layers of anisotropy with a horizontal axis of symmetry.

6. Summary

Relative to NA-SWS-1.1, the spatial coverage for WCUS is dramatically improved in the new database, making it a valuable data set for investigating continental dynamics and evolution. Examples of such applications include (1) joint inversion of surface wave dispersion and SWS data [*Marone and Romanowicz*, 2007; *Yuan and Romanowicz*, 2010a, 2010b]; (2) studying lower mantle anisotropy by removing upper mantle
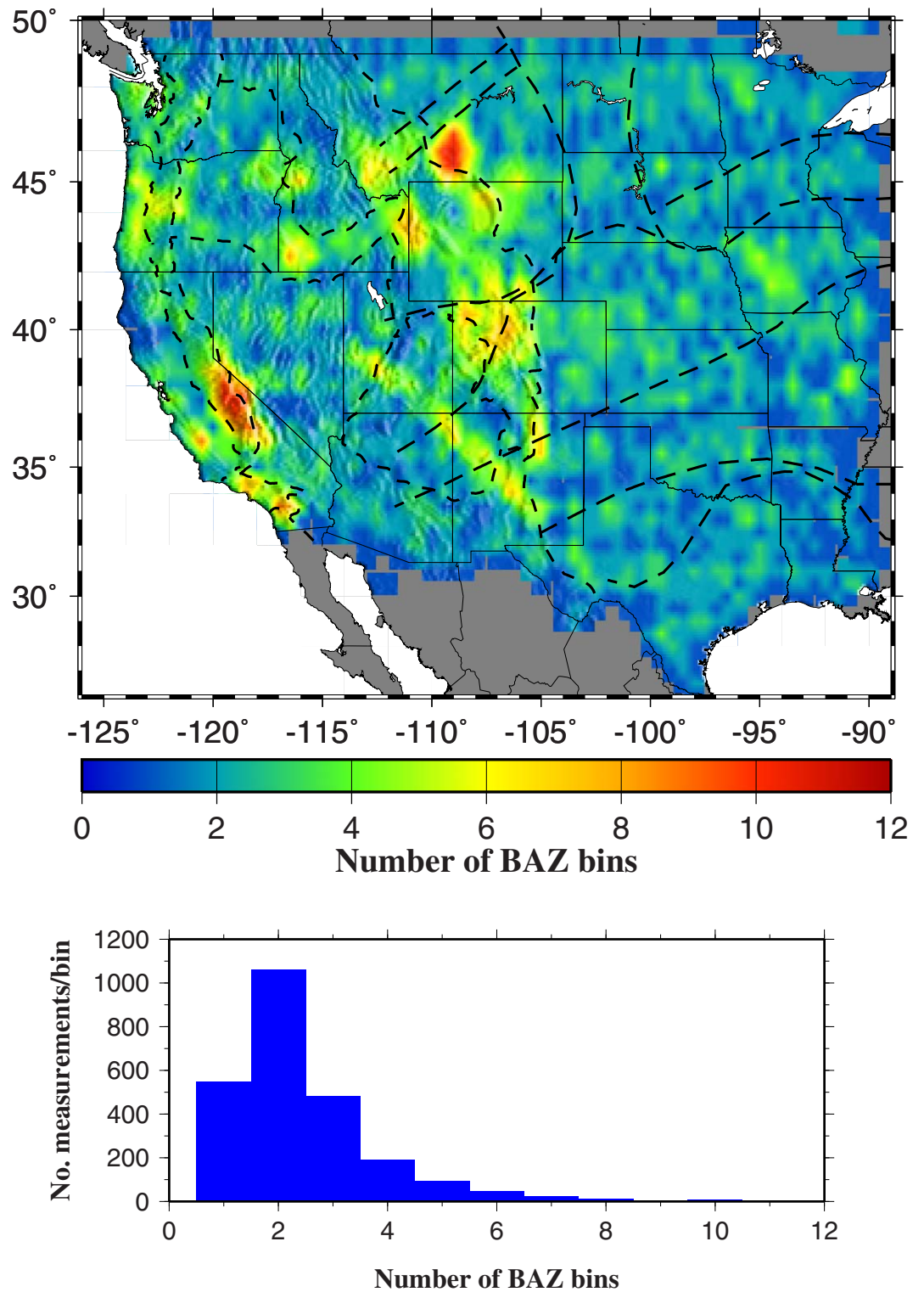
Figure 11. (a) Spatial distribution of the number of back-azimuthal bins. (b) Histogram showing the number of measurements per bin.

anisotropy [*Lay and Garnero*, 2011]; (3) improving seismic tomography results by considering the effects of anisotropy [*van der Lee and Frederiksen*, 2005; *O'Driscoll et al.*, 2011]; (4) investigating the degree of crustal/mantle coupling by comparing GPS-determined surface deformation and SWS-determined mantle
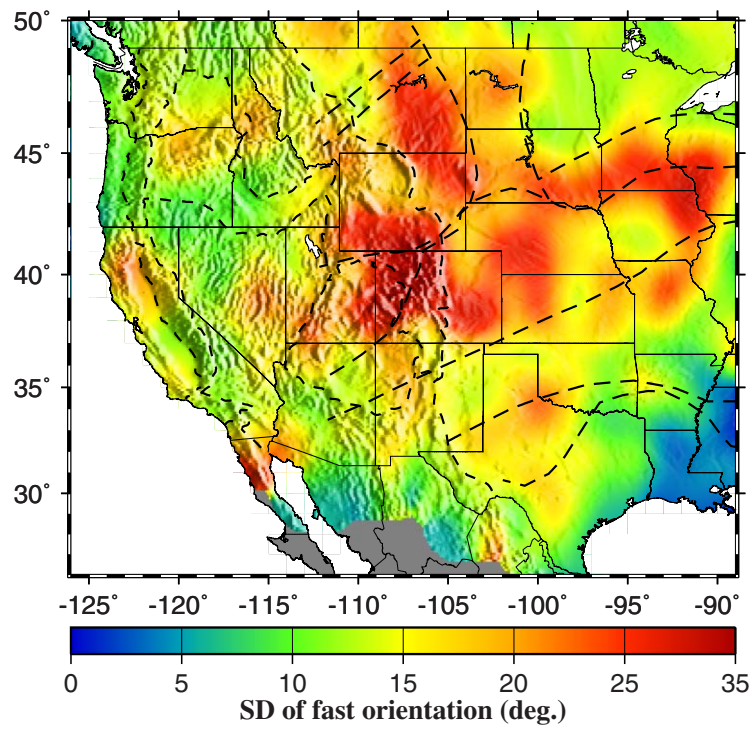
Figure 12. Distribution of the standard deviation of spatially averaged fast orientations. The results plotted were resampled into a resolution of 0.1° and spatially smoothed by a cosine arch filter with a radius of 2°.

deformation [*Flesch et al.*, 2005]; and (5) exploring mantle flow field through geodynamic modeling [*Liu and Bird*, 2002; *Silver and Holt*, 2002; *Becker et al.*, 2006; *Bird et al.*, 2008; *Kreemer*, 2009; *Conrad et al.*, 2007].
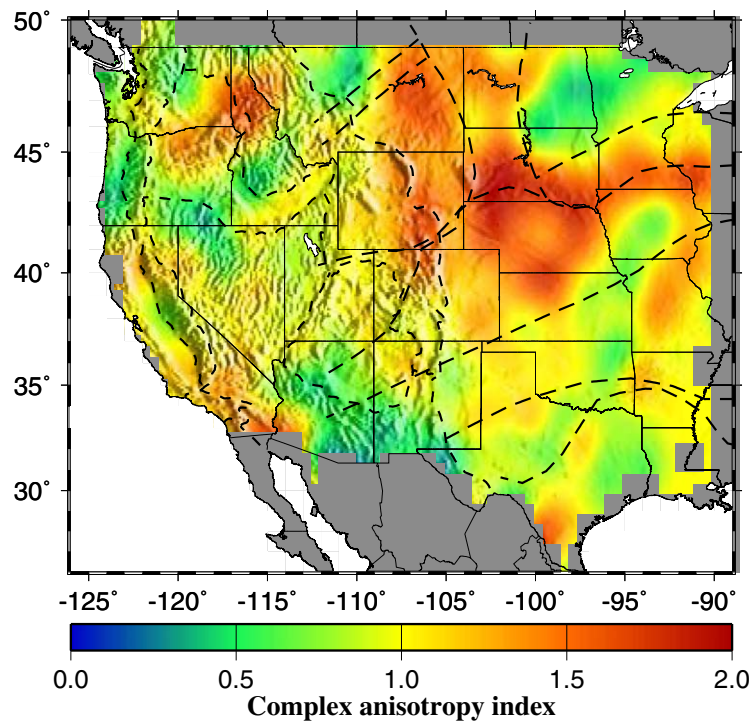
Figure 13. Spatial distribution of complex anisotropy index. The results were smoothed using the same procedure as that used for the previous figure.

At the present time (January 2014), the USArray TA stations are recording in the eastern US; they will be moved to Alaska afterward. Our current plan is to produce the next version of the database by using data from the newly deployed TA and other stations in the eastern US and Alaska.

References

Ando, M., Y. Ishikawa, and F. Yamazaki (1983), Shear wave polarization anisotropy in the upper mantle beneath Honshu, Japan, *J. Geophys. Res.*, *88*, 5850–5864.

Becker, T. W., V. Schulte-Pelkum, D. K. Blackman, J. B. Kellogg, and R. J. O. Connell (2006), Mantle flow under the western United States from shear wave splitting, *Earth Planet. Sci. Lett.*, *247*, 235–251.

Becker, T. W., J. T. Browaeys, and T. H. Jordan (2007), Stochastic analysis of shear-wave splitting length scales, *Earth Planet. Sci. Lett.*, *259*, 526–540.

Bird, P., Z. Liu, and W. K. Rucker (2008), Stresses that drive the plates from below: Definitions, computational path, model optimization, and error analysis, *J. Geophys. Res.*, *113*, B11406, doi:10.1029/2007JB005460.

Conrad, C. P., M. D. Behn, and P. G. Silver (2007), Global mantle flow and the development of seismic anisotropy: Differences between the oceanic and continental upper mantle, *J. Geophys. Res.*, *112*, B07317, doi:10.1029/2006JB004608.

Flesch, L. M., W. E. Holt, P. G. Silver, M. Stephenson, C. Y. Wang, and W. W. Chan (2005), Constraining the extent of crust-mantle coupling in central Asia using GPS, geologic, and shear wave splitting data, *Earth Planet. Sci. Lett.*, *238*, 248–268.

Fuchs, K. (1977), Seismic anisotropy of the subcrustal lithosphere as evidence for dynamical processes in the upper mantle, *Geophys. J. R. Astron. Soc.*, *49*, 167–179.

Gao, S. S., and K. H. Liu (2009), Significant seismic anisotropy beneath the southern Lhasa Terrane, Tibetan Plateau, *Geochem. Geophys. Geosyst.*, *10*, Q02008, doi:10.1029/2008GC002227.

Gao, S. S., K. H. Liu, and M. G. Abdelsalam (2010), Seismic anisotropy beneath the Afar Depression and adjacent areas: Implications for mantle flow, *J. Geophys. Res.*, *115*, B12330, doi:10.1029/2009JB007141.

Gripp, A. E., and R. G. Gordon (2002), Young tracks of hotspots and current plate velocities, *Geophys. J. Int.*, *150*, 321–361.

Kreemer, C. (2009), Absolute plate motions constrained by shear wave splitting orientations with implications for hot spot motions and mantle flow, *J. Geophys. Res.*, *114*, B10405, doi:10.1029/2009JB006416.

Lay, T., and E. J. Garnero (2011), Deep mantle seismic modeling and imaging, *Annu. Rev. Earth Planet. Sci.*, *39*, 91–123.

Liu, K. H. (2009), NA-SWS-1.1: A uniform database of teleseismic shear wave splitting measurements for North America, *Geochem. Geophys. Geosyst.*, *10*, Q05011, doi:10.1029/2009GC002440.

Liu, K. H., and S. S. Gao (2013), Making reliable shear-wave splitting measurements, *Bull. Seismol. Soc. Am.*, *103*(5), 2680–2693, doi:10.1785/0120120355.

Liu, K. H., S. S. Gao, Y. Gao, and J. Wu (2008), Shear wave splitting and mantle flow associated with the deflected Pacific slab beneath northeast Asia, *J. Geophys. Res.*, *113*, B01305, doi:10.1029/2007JB005178.

Liu, Z., and P. Bird (2002), North America plate is driven westward by lower mantle flow, *Geophys. Res. Lett.*, *29*(24), 2164, doi:10.1029/2002GL016002.

Marone, F., and B. Romanowicz (2007), The depth distribution of azimuthal anisotropy in the continental upper mantle, *Nature*, *447*, 198–201.

O'Driscoll, L. J., E. D. Humphreys, and B. Schmandt (2011), Time corrections to teleseismic P delays derived from SKS splitting parameters and implications for western U.S. P-wave tomography, *Geophys. Res. Lett.*, *38*, L19304, doi:10.1029/2011GL049031.

Refayee, H. A., B. B. Yang, K. H. Liu, and S. S. Gao (2013), Mantle flow and lithosphere-asthenosphere coupling beneath the southwestern edge of the North American craton: Constrains from shear-wave splitting measurements, *Earth Planet. Sci. Lett.*, doi:10.1016/j.epsl.2013.01.031.

Savage, M. K., and A. F. Sheehan (2000), Seismic anisotropy and mantle flow from the Great Basin to the Great Plains, western United States, *J. Geophys. Res.*, *105*, 13,715–13,734.

Silver, P. G. (1996), Seismic anisotropy beneath the continents: Probing the depths of geology, *Annu. Rev. Earth Planet Sci.*, *24*, 385–432.

Silver, P. G., and W. W. Chan (1991), Shear wave splitting and subcontinental mantle deformation, *J. Geophys. Res.*, *96*, 16,429–16,454.

Silver, P. G., and W. E. Holt (2002), The mantle flow field beneath western North America, *Science*, *295*, 1054–1057.

Silver, P. G., and M. K. Savage (1994), The interpretation of shear-wave splitting parameters in the presence of two anisotropic layers, *Geophys. J. Int.*, *119*, 949–963.

van der Lee, S., and A. Frederiksen (2005), Surface wave tomography applied to the North American upper mantle, in *Seismic Earth: Array Analysis of Broadband Seismograms, Geophys. Monogr. Ser.*, vol. 157, edited by G. Nolet and A. Levander, pp. 67–80, AGU, Washington, D. C.

Vecsey, L., J. Plomerova, and V. Babuska (2008), Shear-wave splitting measurements-Problems and solutions, *Tectonophysics*, *462*, 178–196.

Vinnik, L. P., L. I. Makeyeva, A. Milev, and A. Y. Usenko (1992), Global patterns of azimuthal anisotropy and deformations in the continental mantle, *Geophys. J. Int.*, *111*, 433–447.

Yang, B. B., S. S. Gao, K. H. Liu, A. A. Elsheikh, A. A. Lemnifi, H. A. Refayee, and Y. Yu (2014), Seismic anisotropy and mantle flow beneath the northern Great Plains of North America, *J. Geophys. Res.* Solid Earth, *119*, doi:10.1002/2013JB010561.

Yuan, H., and B. Romanowicz (2010a), Depth dependent azimuthal anisotropy in the western US upper mantle, *Earth Planet. Sci. Lett.*, *300*, 385–394, doi:10.1016/j.epsl.2010.10.020.

Yuan, H., and B. Romanowicz (2010b), Lithospheric layering in the North American craton, *Nature*, *466*, 1063–1069.